

TransFlower: An Explainable Transformer-Based Model with Flow-to-Flow Attention for Commuting Flow Prediction

Yan Luo
Hong Kong Polytechnic University &
Massachusetts Institute of Technology
China & USA
yluo97@mit.edu

Zhuoyue Wan
Hong Kong Polytechnic University
Hong Kong SAR, China
zhuoyuewan@polyu.edu.hk

Yuzhong Chen
Arizona State University
Tempe, AZ, USA
cyz001383@gmail.com

Gengchen Mai
University of Georgia
Athens, GA, USA
gengchen.mai25@uga.edu

Fu-lai Chung
Hong Kong Polytechnic University
Hong Kong SAR, China
ckschung@polyu.edu.hk

Kent Larson
Massachusetts Institute of Technology
Cambridge, MA, USA
kll@media.mit.edu

ABSTRACT

Understanding the link between urban planning and commuting flows is crucial for guiding urban development and policymaking. This research, bridging computer science and urban studies, addresses the challenge of integrating these fields with their distinct focuses. Traditional urban studies methods, like the gravity and radiation models, often underperform in complex scenarios due to their limited handling of multiple variables and reliance on overly simplistic and unrealistic assumptions, such as spatial isotropy. While deep learning models offer improved accuracy, their “black box” nature poses a trade-off between performance and explainability – both vital for analyzing complex societal phenomena like commuting flows. To address this, we introduce TransFlower, an explainable, transformer-based model employing flow-to-flow attention to predict urban commuting patterns. It features a geospatial encoder with an anisotropy-aware relative location encoder for nuanced flow representation. Following this, the transformer-based flow predictor enhances this by leveraging attention mechanisms to efficiently capture flow interactions. Our model outperforms existing methods by up to 30.8% Common Part of Commuters (CPC), offering insights into mobility dynamics crucial for urban planning and policy decisions. The code is accessible at: <https://github.com/zwanah/TransFlower>

CCS CONCEPTS

• **Applied computing** → *Sociology; Forecasting*; • **Human-centered computing** → **Empirical studies in collaborative and social computing**.

KEYWORDS

Human mobility, Applied computing, Social computing

1 INTRODUCTION

Cities, as the epicenters of economic, social, and cultural activities, play a pivotal role in the evolution of human civilization [6, 7]. Understanding urban human mobility is crucial for creating equitable and sustainable cities, ensuring accessible transportation, economic opportunities, and enhanced quality of life for residents [3, 4, 13]. Commuting flows, defined as the movements between a worker’s

home and their place of employment, play a crucial role in revealing daily movement patterns within urban settings. These flows inform city planning, infrastructure development, and contribute to the understanding of urban dynamics and socioeconomic factors [14, 29]. For instance, some real-world questions we have encountered are, “If a developer plans to introduce several corporate office buildings in a certain area, how would this affect the citywide commuting flows? How should the government appropriately respond by preparing the necessary supporting infrastructure?” If we translate these questions into scientific terminology, they boil down to the problem of commuting flow prediction – learning the correlation between urban planning and the distribution of commuting flows. There are two main practical applications. First, given a new urban development plan, it becomes feasible to determine the corresponding distribution of commuting flows, aiding in the assessment of its impact. Second, traditional methods of collecting commuting flow data rely on national statistical bureaus [23], which are costly and untimely. With a reliable prediction model, we can achieve real-time estimation of commuting flows.

The task of commuting flow prediction sits at the crossroads of urban studies and computer science, each bringing distinct approaches and limitations. Traditionally, urban studies have depended on physical models like the gravity model [5, 11, 30, 38] and radiation model [28] to predict and analyze urban flows, primarily due to limitations in data availability and quantitative analysis capabilities. These models offer a theoretical framework for understanding urban dynamics. However, these models face significant limitations, such as simple assumptions and limited performances [4, 28]. The demand for enhanced performance in this task is crucial, as it allows stakeholders to assess the feasibility of specific planning initiatives and interventions with greater performance. This requirement for performance necessitates access to more comprehensive datasets and a shift away from traditional models towards more sophisticated methodologies. In response to these challenges, deep learning models from computer science have emerged as a powerful alternative [16, 34, 36], offering the promise of higher performance by leveraging large volumes of data to learn complex patterns of urban mobility. Despite their success in achieving improved predictive performance, these models often suffer from a lack of explainability or provide insights that are too shallow for practical application in urban planning. In the context of social phenomena like commuting

flows, the importance of explainability is on par with performance. A thorough understanding of the underlying forces and dynamics of mobility is crucial for validating the model’s credibility and supporting planning and policy development efforts. This opacity poses a dilemma, as there traditionally exists a trade-off between deep learning models’ performance and explainability [9]. Recent advances within the Explainable Artificial Intelligence (XAI) community, however, demonstrate that it is possible to design models that do not sacrifice model explainability for performance [26]. Some works point out that creating an explainable architecture involves designing with explainability in mind, such as utilizing fewer hidden layers or learnable parameters or adopting a modular design, so that every part of the model has a clear function and explanation [2, 12]. Inspired by this development, an intriguing research question emerges: *"How to design a model for commuting flow prediction that achieves both high performance and good explainability?"*

To answer this question, we conducted an in-depth analysis of the two classical models previously mentioned: the gravity model and the radiation model. The gravity model predicts flow distribution by mimicking the gravitational forces observed in the physical world, suggesting that the volume of commuting flow is directly proportional to the attraction between two locations and inversely proportional to the distance between them. Despite its explanatory power through a clear, parameter-based formula, the gravity model’s reliance on region-specific adjustable parameters and known analytical inconsistencies limits its applicability [28]. In response, the radiation model [28] was developed to overcome many of the gravity model’s drawbacks, using a stochastic process to simulate local mobility decisions and analytically deriving commuting and mobility fluxes based on population distribution alone. Nonetheless, the radiation model’s reliance on a limited set of variables (primarily population and distance) results in low performance due to the omission of critical geographical details like land use types and points of interest (POIs). Moreover, it assumes a isotropic ideal space by simple distance decay for flow determinants, disregarding the diverse factors and complex spatial correlations influencing human mobility, such as transportation conditions, topography, and land use patterns, which leads to inaccuracies in representing the actual structure and variability of flows [4]. The limitations of the former can be addressed by integrating comprehensive geographic data of urban regions into deep-learning models, while for the latter, we aim to develop a module within our model capable of adaptively learning location characteristics to circumvent the unrealistic assumption of spatial isotropicity [21, 35, 37].

Additionally, it is worth noting that among the methods involving deep learning, one particular study, DeepGravity [27], touches upon explainability. DeepGravity claims to provide explainability through SHAP [17], a game theory-based approach for interpreting machine learning models. However, such model-agnostic explanation methods can only superficially mimic the input-output relationship of the actual model, without the ability to deeply analyze causal relationships. A fundamental reason for the lack of deep explainability for DeepGravity is the oversimplified modeling that relies solely on feed-forward networks to encode information from individual flows, thereby overlooking the interplay between

flows. Given that commuting flows represent a complex network challenge, understanding the intricate dynamics and interplay between flows is crucial. These interactions are key to deciphering the mechanisms of information transmission within the network and understanding how the network’s structure impacts these processes [10]. Therefore, incorporating interactions between flows could not only enhance the model’s explainability but also potentially contribute to an improvement in performance.

In light of these considerations, we have approached the design of our solution from first principles, resulting in the creation of a minimalist yet effective model. We introduce TransFlow, an explainable transformer-based [32] model featuring flow-to-flow attention mechanisms specifically tailored for the predicting of commuting flows. The transformer is selected primarily for its efficiency in handling the interactions among items within a sequence or a set, enabling intricate flow relationships to be modeled. Additionally, the attention mechanism enhances model explainability. Specifically, we first employ a novel relative location encoder to capture the spatial relationship between the origin and destination regions of individual flows. While the DeepGravity model only considers the distance between origins and destinations, with the help of relative location encoding, our model can jointly consider both distance and direction information. This encoder is designed to adaptively learn spatial representations, effectively countering the radiation model’s unrealistic assumption of spatial uniformity and isotropicity. Subsequently, we integrate the spatial relationship information with other geographic features of the flow’s origin and destination regions in the geo-spatial encoder. This integrated data is then fed into a transformer-based flow predictor designed to learn the interactions between different flows. Finally, we utilize attention mechanisms between flows to investigate the relationship between commuting flows and urban features, offering new insights into the dynamics of urban mobility.

Our experiments, conducted across three states in the US, indicate that our framework outperforms existing state-of-the-art deep learning models by up to 30.8% in terms of the metric Common Part of Commuters (CPC). Additionally, we illustrate how the flows generated by our model can be explained through flow-to-flow attention mechanisms. Moreover, we prove that our relative location encoder is capable of capturing spatial anisotropicity. With our model, stakeholders will be equipped to precisely describe the dynamics of commuting flows, a crucial aspect in shaping cities in alignment with SDGs.

2 PROBLEM FORMULATION

It is noteworthy that the prediction of commuting flows differs from the more common spatiotemporal traffic flow forecasting problem [15, 33]. Traffic flow is a short-term, dynamic, and time-series-related phenomenon, whereas commuting flows represent long-term, relatively static, and time-series-independent repeated daily movements. In traffic flow modeling, historical flows are used as input features, whereas the inputs for commuting flow prediction problems are the geographical attributes of urban regions.

Definition 1 Urban Region: Urban regions u_i can be census blocks, block groups, census tracts, counties, or states. To ensure

our model has an appropriate number of samples in each experimental area, in this paper, we use block groups as urban regions. Each region is characterized by a variety of geo-spatial features, including place features (e.g., POIs within the region) and location information. Place features of each region can be represented as x_{u_i} . The centroid coordinates of each region can be indicated by loc_{u_i} . The distance measured along the surface of the earth between the centroid of region u_i and region u_j is denoted as r_{ij} .

Definition 2 Commuting Flow: Commuting flows are a set of 3-tuple $f_{ij} = (o_i, d_j, v_{ij})$ where o_i is the flow origin urban region, d_j is the flow destination urban region, v_{ij} is the number of commuters moving from o_i to d_j per unit time. We use $S = \{f_{kl} = (o_k, d_l, v_{kl})\}$ to denote the full set of all urban commuting flows and $S_i = \{f_{il} = (o_i, d_l, v_{il})\} \subseteq S$ be the subset of S denoting all flows originating from region o_i . Then the total outflow, O_i , from region o_i is the total number of flows per unit time originating from region o_i , i.e., $O_i = \sum_{f_{il} \in S_i} v_{il}$.

Problem Statement Commuting Flow Prediction: Essentially, this can be considered a task of outflow allocation. We can first forecast the probabilities of destinations for flows originating from a specific origin region. By multiplying these predicted probabilities with the known outflows, we can determine the actual flows.

3 METHODOLOGY

Considering the geo-spatial features x_{u_i} and loc_{u_i} of urban regions, the output of TransFlower is an n -dimensional vector $P_{i,j}$, where $j = 1, \dots, n$, representing the probability of flows originating from o_i and arriving at each destination d_j . As illustrated in Figure 1, the model employs two major components to achieve this: the geo-spatial encoder and the flow predictor.

3.1 Geo-Spatial Encoder

Predicting commuting flows fundamentally involves geo-spatial information. To this end, we introduce the Geo-Spatial Encoder. The input to the Geo-Spatial Encoder is divided into three main categories: the place features x_{u_i} of both the origin and destination regions, the coordinate information loc_{u_i} of these regions, and the distance r_{o_i, d_j} between them. Following the practice of DeepGravity [27], we concatenate the place features of the origin and destination, i.e., x_{o_i} and x_{d_j} , as well as the distance r_{o_i, d_j} , and feed these features to a feed-forward neural network to obtain an embedding capturing the characteristics of both o_i and d_j .

However, merely accounting for the distance r_{o_i, d_j} falls short of capturing comprehensive spatial information, as commuting flows exhibit anisotropic patterns [35], indicating that direction is also a crucial piece of information to consider. Thus, we compute the relative location $rl_{ij} = loc_{o_i} - loc_{d_j} (\in \mathbb{R}^2)$ and feed it into a specially designed relative location encoder based on Space2Vec [22], to jointly capture the distance and direction information.

3.1.1 Geographic Feature Encoder. To extract information on individual flows, we follow the practice of benchmark model DeepGravity, by using place features and the distance feature as inputs for our flow geographic feature encoder.

Place features, denoted by x_{u_i} (u_i can be either o_i or d_j), delineate various geographical aspects of areas, such as the number of

retail establishments present within a specific region. The dimensionality of these place features corresponds to the aggregate count of features evaluated. Among the place features utilized are the population magnitude of each region and 19 attributes derived from OpenStreetMap [24], spanning the following categories:

- Facilities related to food (4 attributes: point-amenity, point-shop, polygon-amenity, polygon-shop): the comprehensive tally of POIs and structures associated with any food-related service, e.g., restaurants, fast food outlets, and bars.
- Facilities related to retail (4 attributes: point-amenity, point-shop, polygon-amenity, polygon-shop): the comprehensive tally of POIs and structures associated with retail services, e.g., marketplaces, pharmacies, and convenience stores.
- Facilities related to education (3 attributes: point-amenity, polygon-amenity, polygon-building): the comprehensive tally of POIs and structures associated with educational institutions, e.g., schools, colleges, and universities.
- Facilities related to health (3 attributes: point-amenity, polygon-amenity, polygon-building): the comprehensive tally of POIs and structures associated with health services, e.g., dentists, hospitals, and clinics.
- Facilities related to transport (5 attributes: point-amenity, point-public-transport, polygon-amenity, polygon-building, polygon-public-transport): the comprehensive tally of POIs and structures associated with transport services, e.g., parking lots, bus stations, and charging stations.

We concatenate the distance feature $r_{i,j}$ with a 40-dimensional vector of place features, x_{u_i} , which includes 19 geographic attributes from both the origin and destination, in addition to their respective population counts, to formulate the 41-dimensional feature embedding that define individual flow patterns. These consolidated features are then subjected to a transformation through a single-layer feed-forward network, resulting in a 256-dimensional individual flow representation x_{o_i, d_j} . This process effectively projects the lower-dimensional features into a higher-dimensional space.

3.1.2 Relative Location Encoder. To overcome the unrealistic assumption of spatial isotropicity in classical models, we introduce a relative location encoder to adaptively learn the representation of spatial information for each flow. While there has been some work on spatial representation learning [18, 19], most of it deals with specific tasks and often disregards geographic coordinates. Space2Vec [22] is a general-purpose representation learning model that encodes the absolute positions or spatial relationships of places into a vector space representation. This work is inspired by the Nobel Prize-winning neuroscience research that demonstrated mammalian grid cells provide a multi-scale periodic representation [1]. It has been discovered that leveraging location embeddings, generated through coordinate decomposition, assists deep-learning models in overcoming the limitations inherent in traditional single-scale approaches by adopting multi-scale representations [20].

Inspired by the multi-scale representations of Space2Vec, we develop a relative location encoder that comprises two key components: a multi-scale encoder and a feed-forward network. Unlike Space2Vec, which operates on single coordinate points, our focus is on flow. We calculate the relative location $rl_{ij} = loc_{o_i} - loc_{d_j}$ as the inputs for our relative location encoder.

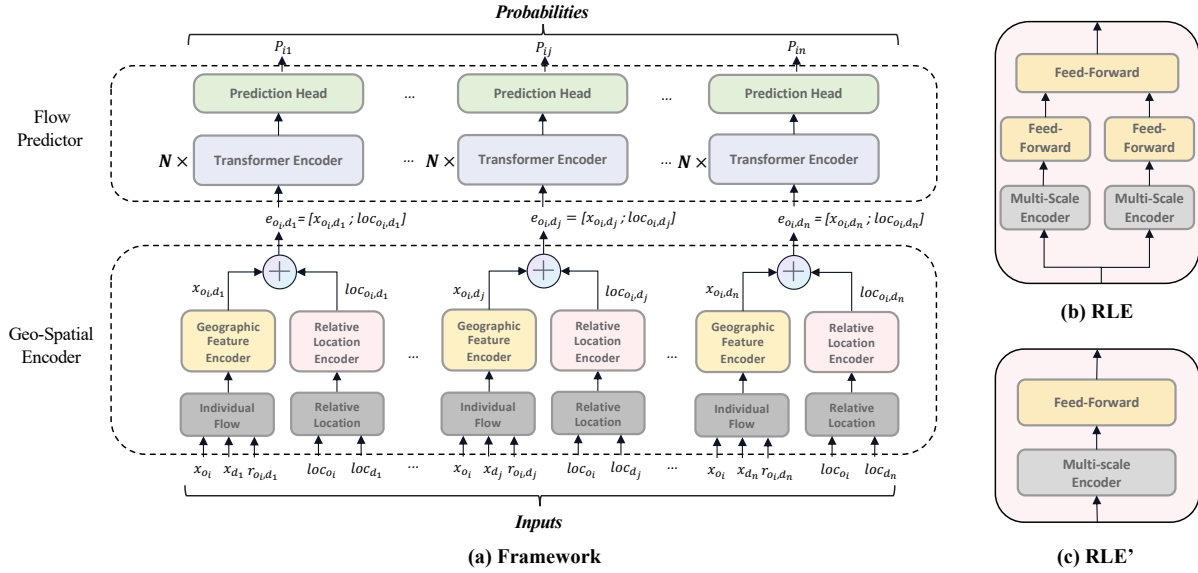


Figure 1: The framework of TransFlower which contains two major components: geo-spatial encoder and flower predictor.

More precisely, our relative location encoder represents the relative location rl_{ij} in a multi-scale relative location embedding. While traditional transformer position encoding layers operate in discrete 1-dimensional spaces, such as word positions in a sentence, we tackle higher-dimensional continuous spaces, like the Earth’s surface. To encompass a 2-dimensional space, we utilize a set of sine and cosine functions at various frequencies, amounting to $freq$ in total, to encode the relative location rl_{ij} . The multi-scale encoder is denoted as $Enc(rl_{ij}) = NN(PE(rl_{ij}))$, where NN consists of fully connected ReLU layers. Here, $PE(rl_{ij}) = [PE_0(rl_{ij}); \dots; PE_{K-1}(rl_{ij})]$ concatenates multi-scale representations. K is the total number of scales.

We decompose and project the relative location rl_{ij} into the direction of three base vectors in \mathbb{R}^2 , named a_1, a_2, a_3 , each distinctly angled at $2\pi/3$ from one another. According to Space2Vec, a typical configuration might set $a_1 = [1, 0]^T$, $a_2 = [-1/2, \sqrt{3}/2]^T$, and $a_3 = [-1/2, -\sqrt{3}/2]^T$, establishing a symmetrical geometric structure for spatial encoding. λ_{min} and λ_{max} represent the minimum and maximum scales, respectively, with $g = \frac{\lambda_{max}}{\lambda_{min}}$. For each scale s , $PE_s(rl_{ij})$ combines three components as follows:

$$PE_{s,j}(rl_{ij}) = \left[\cos\left(\frac{\langle rl_{ij}, a_j \rangle}{\lambda_{min} \cdot g^{s/(S-1)}}\right); \sin\left(\frac{\langle rl_{ij}, a_j \rangle}{\lambda_{min} \cdot g^{s/(S-1)}}\right) \right], \forall j = 1, 2, 3; \quad (1)$$

where $\langle rl_{ij}, a_j \rangle$ is the inner product of rl_{ij} and a_j .

It’s noteworthy that an analysis of Figure 2d revealed intriguing experimental phenomena (to be detailed in Section 4.4), prompting a reevaluation of the design of the relative location encoder. We proposed two designs for the Relative Location Encoder (RLE):

- **RLE**: As shown in Figure 1b, the encoder includes two branches, each with a multi-scale encoder and a feed-forward network. Two encoders have distinct base vector sets. An additional feed-forward layer merges outputs from both

branches, creating loc_{o_i, d_j} which captures the complex geographical relationships between origin and destination regions at multiple levels.

- **RLE'**: Illustrated in Figure 1c, this encoder variant operates with a single branch, utilizing the typical configuration of base vectors’ orientations as mentioned above. The output from this branch, loc_{o_i, d_j} , is the relative location vector.

Subsequently, by concatenating the individual flow embedding x_{o_i, d_j} with the flow spatial embedding loc_{o_i, d_j} generated by the relative location encoder, we create a comprehensive embedding for each flow, represented as $e_{o_i, d_j} = [x_{o_i, d_j}; loc_{o_i, d_j}]$. This process effectively combines specific flow characteristics with spatial information, facilitating a more nuanced analysis of commuting patterns.

3.2 Flow Predictor

In the flow predictor, the generated flow embeddings from the geo-spatial encoder are processed through a N -layer transformer encoder module to model the interactions among different flows that share the same origin with the self-attention mechanism. This is followed by a prediction head, which includes a feed-forward layer and a softmax layer, to generate the probability distribution of flows from a specified origin region to various destination regions. This structure ensures that the model captures the complex dynamics and interactions between different commuting flows, enhancing its predictive performance and relevance for urban planning and analysis.

3.2.1 Transformer Encoder. Our choice of a transformer-based model is grounded in its sequential processing capabilities, allowing for effective representation of flow relationships and complex mobility patterns. Its attention mechanism offers explicit input prioritization and improved explainability through visual insights

into predictive focuses. Furthermore, transformers’ contextual processing and parallelism enhance efficiency, making them ideal for large-scale and complex commuting flow analyses.

Specifically, each transformer encoder layer consists of a multi-head self-attention module and a feed-forward network. Residual connections and layer normalizations are also employed. In each attention head, self-attention for flow f_{ij} can be formulated as:

$$e_{i'} = e_i + w_z \sum_{j=1}^n \frac{\exp(w_q e_i \times w_k e_j)}{\sum_{m=1}^n \exp(w_q e_i \times w_k e_m)} w_v e_j \quad (2)$$

where e_i and $e_{i'}$ are the input and output embeddings, and $w_{\{q,k,v,z\}}$ denotes linear transform weights for the query, key, value, and output matrices.

3.2.2 Prediction Head. The outputs from transformer encoder layers are then fed into a feed-forward layer, which leads to a score $s(o_i, d_j)$ ranging from $-\infty$ to $+\infty$. For any region pair (o_i, d_j) , a higher score indicates a greater likelihood of observing a flow from o_i to d_j . Subsequently, a softmax function converts these scores into probabilities $P_{i,j}$, ensuring they are positive and collectively sum to one. The actual flow between two regions is then determined by multiplying this probability with the total outflow from the origin region.

3.2.3 Loss Function. The model’s loss function is defined as cross-entropy, as it measures the difference between the predicted probabilities and the actual distribution, effectively guiding the model to improve its predictions over time. The loss can be denoted as:

$$H = - \sum_i \sum_j \frac{f_{ij}(o_i, d_j)}{O_i} \ln P_{i,j} \quad (3)$$

where $\frac{f_{ij}(o_i, d_j)}{O_i}$ represents the proportion of observed flows departing from origin o_i to destination d_j , while $P_{i,j}$ signifies the predicted probability by the model for a flow from o_i to d_j . The aggregation of cross-entropy values across different origins, denoted by the sum over i , is based on the premise that flows originating from disparate locations are considered independent events. This assumption enables the utilization of cross-entropy’s additive nature for independent variables, facilitating a comprehensive evaluation of the model’s performance across multiple origins.

4 RESULTS

In this section, we conduct extensive experiments on three datasets to evaluate our proposed model.

4.1 Experiment Setups

4.1.1 Datasets. We evaluated our proposed model on real-world commuting flow datasets collected from California, Massachusetts, and Texas. Our input data for urban regions was sourced from the 2019 American block group’s cartographic boundary files provided by the US Census Bureau. Due to computational considerations, we selectively focused on specific areas within California (7872 block groups), Massachusetts (2350 block groups), and Texas (7900 block groups), ensuring coverage of the most central and significant locations. For instance, the regions selected in California include key areas such as Los Angeles and San Francisco, highlighting

our model’s applicability to diverse and densely populated urban environments.

For commuting flows, we utilized the 2019 Origin-Destination Employment Statistics (LODES) dataset [31]. This dataset is updated annually and captures the home and employment locations of workers, thus offering insights into stable commuting patterns. The commuting flows are then aggregated to the geographic unit level for analysis. In our experimental area in California, a total of 2,552,243 origin-destination pairs accounted for 5,583,372 commuting flows. The Massachusetts dataset included 58,235 origin-destination pairs, leading to 1,404,860 commuting flows. In Texas, there were 756,179 origin-destination pairs, resulting in 1,688,550 commuting flows.

For place attributes, we employ point and polygon data from OpenStreetMap [24], a widely recognized platform for volunteer-contributed geographic information. Each point and polygon represents a geographic feature with a specific purpose. Typically, a polygon is used to delineate the outline of a building. For example, Union Station could be depicted as either a point or a polygon, categorized under public transportation. Conversely, a restaurant located within Union Station would be represented as an independent point separate from Union Station, and it would fall under the category of dining.

4.1.2 Evaluation Metrics. To evaluate the performance of our predictions, we utilize three widely recognized metrics: Common Part of Commuters (CPC), Mean Absolute Error (MAE), and Root Mean Squared Error (RMSE) [4, 27]. MAE and RMSE offer a straightforward and effective means of assessing the magnitude of errors in regression analyses. CPC quantifies the similarity between the predicted flow volume $v^p(o_i, d_j)$ and real flow volume $v^r(o_i, d_j)$, which can be denoted as:

$$CPC = \frac{2 \sum_{i,j} \min(v^p(o_i, d_j), v^r(o_i, d_j))}{\sum_{i,j} v^p(o_i, d_j) + \sum_{i,j} v^r(o_i, d_j)}. \quad (4)$$

4.1.3 Implementations. To align with the settings used in DeepGravity, we randomly partition the commuting flows into training and validation datasets using an 80:20 split. The network training employs the early stopping technique to prevent overfitting, with a patience setting of 20 epochs and utilizes the RMSprop optimizer. This optimizer is configured with a momentum of 0.9 and a learning rate of 0.0001, processing batches containing 512 origin regions each. The feed-forward network features a hidden size of 256, and we set the network’s random seed to 1234. A dropout rate of 0.1 is applied to mitigate overfitting, and the Transformer encoder is structured with two layers.

To streamline the training process of the transformer and ensure alignment with DeepGravity’s methodology, we select 256 destination regions for each origin region. This number approximates the average count of flows originating from each region. If the actual number of destinations surpasses 256, we employ random sampling to select 256 destinations; Otherwise, we utilize zero-padding to achieve this count.

Regarding the parameters within the relative location encoder, the maximum lambda λ_{max} is set to the maximum diameter of

the study area, which is 20013 m for California, 20009 m for Massachusetts, and 20013 m for Texas. The number of different sinusoidal with different frequencies $freq$ and minimum scale λ_{min} are hyperparameters, optimized differently across study areas. For instance, for the California dataset, $freq$ is set to 16, and the λ_{min} to 1.

4.1.4 Baselines. To demonstrate our model’s efficacy, we conduct comparisons against the following baseline models:

- Gravity [4]: This adaptation of the classic gravity model incorporates two power exponents, suggesting that the flow of people or goods between two areas directly correlates with their propulsiveness (outflow) and attractiveness (inflow), while being inversely related to the distance separating them. The model’s inputs exclude geographic features.
- Radiation [28]: The radiation model posits that urban mobility is determined by the city’s population density distribution. The likelihood of movement from origin o_i to destination d_j is denoted by the following formulation:

$$P_{i,j} = \frac{p_i p_j}{(p_i + S_{i,j})(p_i + p_j + S_{i,j})} \quad (5)$$

where p_i represents the population of the origin region o_i , and $S_{i,j}$ denotes the total population within the circle centered at o_i with a radius equal to the distance between the origin and destination. The model’s inputs exclude geographic features.

- Random Forest (RF) [25]: As a classical machine learning method [8], RF is reported as a strong baseline [25]. The inputs are consistent with ours.
- GMEL [16]: This model forms an adjacency graph and utilizes two attention-based graph neural networks (GATs) to independently learn the embeddings for origins and destinations. Additionally, the authors designed two supplementary tasks for forecasting inflow and outflow. To make a fair comparison with our model, we did not adopt this supplementary part. The inputs are consistent with ours.
- DeepGravity [27]: This model views flow prediction as a task of allocating outflow and forecasts the probabilities of destinations for flows originating from a specific origin region. The inputs are consistent with ours.

4.2 Performance Analysis

We evaluated the performance of both baseline models and our proposed model using a test set, with detailed results presented in Table 1. TransFlower stands out as the top performer across all datasets and metrics, achieving up to a 30.8% improvement on CPC, thereby affirming the effectiveness of our approach. Our analysis offers several key insights.

Among the models assessed, the Radiation model ranks lowest in performance. This shortfall is likely due to its oversimplified assumptions like spatial anisotropy. Conversely, models incorporating geographic features (i.e., RF, GMEL, DeepGravity, TransFlower) markedly surpass those lacking these elements (i.e., Gravity and Radiation). This finding emphasizes the critical role of geographic features in the accurate prediction of commuting flows. By embedding spatial contextual information, these models gain a nuanced

Table 1: Performance analysis

| Dataset | Model Name | CPC | MAE | RMSE |
|---------------|-------------|---------------|---------------|---------------|
| California | Gravity | 0.6847 | 1.1626 | 3.5443 |
| | Radiation | 0.4074 | 2.0782 | 6.4025 |
| | RF | 0.6451 | 1.2987 | 3.2309 |
| | DeepGravity | 0.6571 | 1.2475 | 3.1099 |
| | GMEL | 0.6533 | 1.2563 | 3.1407 |
| | TransFlower | 0.7691 | 0.8380 | 2.0780 |
| Massachusetts | Gravity | 0.6403 | 1.5147 | 3.5032 |
| | Radiation | 0.3221 | 2.6807 | 6.2174 |
| | RF | 0.6829 | 1.4343 | 3.0398 |
| | DeepGravity | 0.6871 | 1.4151 | 2.9036 |
| | GMEL | 0.6831 | 1.4347 | 2.9233 |
| | TransFlower | 0.7573 | 1.0980 | 2.2700 |
| Texas | Gravity | 0.5886 | 1.7434 | 6.1830 |
| | Radiation | 0.3060 | 2.6764 | 7.2387 |
| | RF | 0.4811 | 0.6517 | 3.0475 |
| | DeepGravity | 0.4786 | 0.6819 | 3.0313 |
| | GMEL | 0.4535 | 0.6942 | 3.0753 |
| | TransFlower | 0.6262 | 0.4794 | 2.3590 |

understanding and depiction of commuting flow dynamics, resulting in enhanced performance across a variety of test scenarios.

TransFlower’s superiority over the Gravity model demonstrates how a relative location encoder, capable of assimilating spatial anisotropy, combined with a sophisticated neural network framework, can significantly improve commuting flow prediction performance. Its advantage over DeepGravity further accentuates the value of capturing flow interactions via transformer encoder layers. Additionally, TransFlower outperforms GMEL, a model leveraging GAT, indicating that transformers’ implicit approach to modeling flow relationships is more efficacious than GAT’s explicit method based on geographical proximity. This suggests that in the complex network challenge of commuting flows, the interplay between flows is influenced not solely by geographical proximity but also by complex, latent higher-order relationships.

4.3 Ablation Study

As shown in Table 2, we validate the effectiveness of the key components contributing to performance enhancement: the transformer module and the relative location encoder (RLE). We tested three variants of TransFlower to confirm this: (1) without RLE, (2) with RLE’, and (3) without the transformer module (i.e., DeepGravity with RLE). The experimental results indicate that removing the RLE leads to a minimum drop of 9.7% in CPC.

4.4 Residual Analysis

Taking the experimental area in California as an example, as depicted in Figure 2, we aimed to further assess the effectiveness of various components of our model. We achieved this by analyzing the relative spatial distribution of the differences between the predicted and actual commuting flows and comparing different models or variants of the model through subtraction.

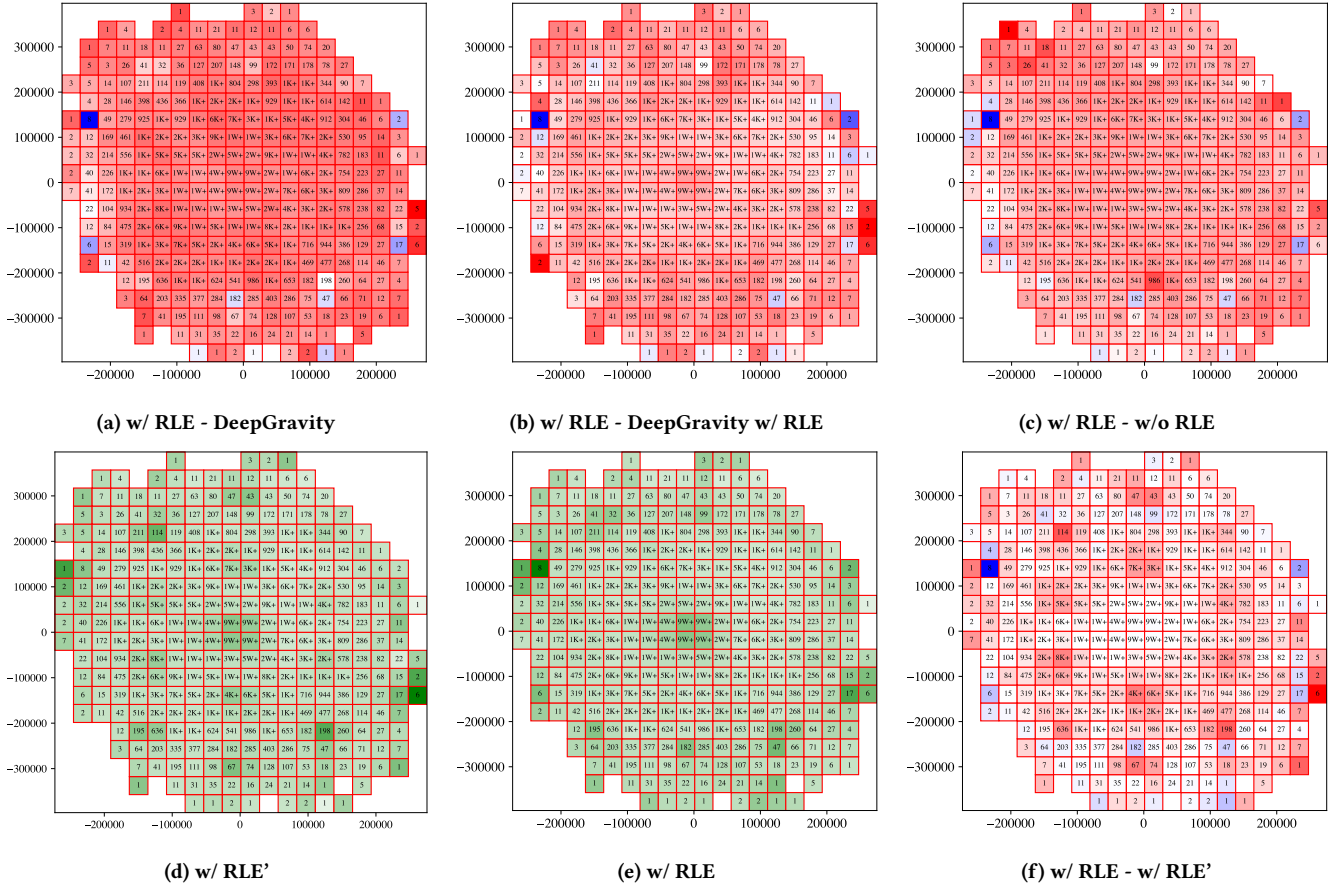


Figure 2: Comparison between different modules.

Table 2: Ablation Study

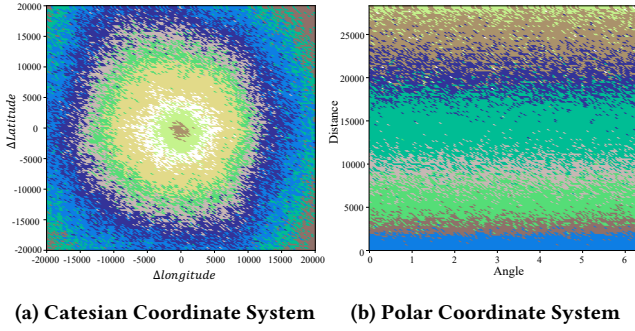
| Dataset | Model Name | CPC | MAE | RMSE |
|---------------|--------------------------|---------------|---------------|---------------|
| California | DeepGravity w/ RLE | 0.7337 | 0.9779 | 2.4580 |
| | w/o RLE | 0.6820 | 1.1491 | 2.8219 |
| | w/ RLE [†] | 0.7602 | 0.8708 | 2.1120 |
| | w/ RLE (i.e., TransFlow) | 0.7691 | 0.8380 | 2.0780 |
| Massachusetts | DeepGravity w/ RLE | 0.7333 | 1.2060 | 2.3950 |
| | w/o RLE | 0.6905 | 1.3997 | 2.8613 |
| | w/ RLE [†] | 0.7499 | 1.1310 | 2.3190 |
| | w/ RLE (i.e., TransFlow) | 0.7573 | 1.0980 | 2.2700 |
| Texas | DeepGravity w/ RLE | 0.5837 | 0.5339 | 2.5580 |
| | w/o RLE | 0.4990 | 0.6265 | 2.8168 |
| | w/ RLE [†] | 0.6104 | 0.4959 | 2.4440 |
| | w/ RLE (i.e., TransFlow) | 0.6262 | 0.4794 | 2.3590 |

We started by organizing the comprehensive dataset of commuting flows based on their relative locations, subsequently dividing these into distinct cells. In this study, the data was segmented into cells measuring 20 by 20 meters. Within each cell, we calculated the average residual value. This involved first identifying the difference between the actual and predicted values for two models being compared, such as model A and model B, within the spatial

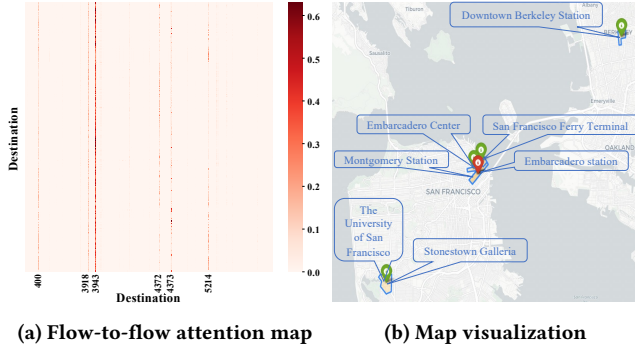
extent of that cell. We then subtracted the residual value of model A in that cell from model B's value and computed their average. This residual value difference is represented by color. Red indicates a positive residual value, meaning model A performs better than model B within that relative spatial range. Conversely, blue indicates a negative residual value, where model A performs worse than model B. The deeper the color, the greater the absolute value of the performance difference is.

Figure 2a essentially illustrates the performance improvement brought by the combined effect of the transformer and RLE modules. Figure 2b underscores the contribution of the transformer to performance improvement, while Figure 2c focuses on the performance enhancement attributed to the RLE alone. It is evident that our proposed modules enhance performance across almost all relative spatial ranges, with a few exceptions in cells at great relative distances, which have very few flows, often in single digits, and can be considered outliers.

Moreover, we further explore the performance differences between two types of relative location encoders. Figure 2d shows the residual map of true versus predicted values using RLE[†], where darker green cells indicate poorer performance in predicting flows from their origins to destinations within that spatial range, with



(a) Cartesian Coordinate System (b) Polar Coordinate System
Figure 3: Location embedding clustering of the relative location encoder from the trained TransFlower.



(a) Flow-to-flow attention map (b) Map visualization
Figure 4: Case study for flow prediction of one origin region in San Francisco.

lighter green cells indicating smaller differences. The areas of deeper blue are roughly distributed at the vertices of a hexagon, which is an artifact created due to the use of 3 base vectors oriented $2\pi/3$ apart from each other. Therefore, to enhance performance and correct this artifact, we experimented with introducing an additional set of base vectors rotated by a certain angle, constructing the RLE. The residual map, as shown in Figure 2e, visibly eliminates the hexagonal pattern. Figure 2f, depicting the difference between RLE and RLE', further validates our hypothesis.

4.5 Explainability Analysis

Grasping the rationale behind a model's prediction is essential for interpreting outcomes, elucidating disparities among models, and gauging our comprehension of the phenomenon being studied.

Our model is elucidated through two primary aspects: Firstly, we investigate the patterns learned by our specially designed relative location encoder, as evidenced by the clustering effectiveness of the generated embeddings. Secondly, we delve into the interpretation of the significance encapsulated within the flow-to-flow attention mechanism.

4.5.1 Location Embedding Clustering. We extracted the RLE from the trained TransFlower to investigate how it functions. Starting with the maximum diameter λ_{max} of the study area, we determined the range for visualizing coordinates to be between $[-\lambda_{max}, \lambda_{max}]$. Taking California as an example, where $-\lambda_{max} = 20013$, the range of both longitude and latitude in the Cartesian coordinate system, as shown in Figure 3, spans from $[-20013, 20013]$.

We then divided this range into 100 equal intervals, creating a grid of 100×100 cells. The coordinate ranges of these 100×100 cells were fed as inputs into the previously trained RLE to generate embeddings for each cell. Subsequently, we applied a hierarchical clustering algorithm to cluster the cells, opting for a 10-category classification and assigning different colors to different categories. To enhance clarity, we also performed visualization in polar coordinates. Figure 3a demonstrates that the clusters of location embeddings primarily form based on their relative distance. However, there is also a subtle variation in clustering by direction, as evidenced by the clusters not forming perfect concentric rings. This indicates that the embeddings obtained from the relative location encoder are anisotropy-aware and capable of capturing both direction and distance.

4.5.2 Flow-to-Flow Attention Map. To gain deeper insights into what the model learns from the interactions between flows, we created a flow-to-flow attention map. We select an origin region in San Francisco as an example, for which the 256 predicted destinations formed a 256×256 attention matrix. The sum of each row in this matrix equals 1. As depicted in Figure 4a, we visualize this matrix where the y-axis represents the destinations, the x-axis denotes the regions influencing the predicted probability of these destinations, and the color intensity signifies the attention values. The darker red points indicate that the x-axis region has a more significant influence on the flow prediction for the y-axis corresponding destination region. Remarkably, the map displays several vertical red lines, suggesting that some regions consistently have a substantial impact on the flow predictions for that origin region.

Naturally, we seek to further investigate what these influential regions correspond to. As shown in Figure 4b, we mark these regions on the map: the origin region in a red icon and the significantly influential regions in green icons. It is observed that these regions carry distinct significance, such as the central business district, the train station, downtown Berkeley, and the University of San Francisco. This demonstrates that our model has learned physically meaningful attention patterns, further emphasizing the critical role of flow interactions in predicting commuting flows.

5 CONCLUSION

This paper tackles the challenge of predicting commuting flows, crucial for urban planning and policymaking. Traditional models like the gravity model and radiation model fall short due to complex variables, whereas deep learning models often compromise explainability for performance. We introduce TransFlower, a transformer-based approach with flow-to-flow attention for precise flow predictions. It features an anisotropy-aware geo-spatial encoder for detailed flow analysis, processed by a transformer with flow-to-flow attention to understand flow interactions. TransFlower excels in both explainability and performance, paving the way for more informed and effective urban development strategies.

REFERENCES

- [1] Alison Abbott and Ewen Callaway. 2014. Nobel prize for decoding brain's sense of place. *Nature News* 514, 7521 (2014), 153.
- [2] Amina Adadi and Mohammed Berrada. 2018. Peeking Inside the Black-Box: A Survey on Explainable Artificial Intelligence (XAI). *IEEE Access* 6 (2018), 52138–52160. <https://doi.org/10.1109/ACCESS.2018.2870052>

- [3] Laura Alessandretti. 2022. What human mobility data tell us about COVID-19 spread. *Nat. Rev. Phys.* 4 (2022), 12–13.
- [4] Hugo Barbosa, Marc Barthélemy, Gourab Ghoshal, Charlotte R James, Maxime Lenormand, Thomas Louail, Ronaldo Menezes, José J Ramasco, Filippo Simini, and Marcello Tomasini. 2018. Human mobility: Models and applications. *Physics Reports* 734 (2018), 1–74.
- [5] Marc Barthélemy. 2011. Spatial networks. *Physics reports* 499, 1-3 (2011), 1–101.
- [6] Michael Batty. 2013. *The New Science of Cities*. The MIT Press.
- [7] Luis MA Bettencourt, José Lobo, Dirk Helbing, Christian Kühnert, and Geoffrey B West. 2007. Growth, innovation, scaling, and the pace of life in cities. *Proceedings of the national academy of sciences* 104, 17 (2007), 7301–7306.
- [8] Leo Breiman. 2001. Random forests. *Machine learning* 45 (2001), 5–32.
- [9] Defense Advanced Research Projects Agency. 2016. Broad Agency Announcement, Explainable Artificial Intelligence (XAI). DARPA-BAA-16-53. <https://www.darpa.mil/attachments/DARPA-BAA-16-53.pdf>
- [10] Reik V Donner, Emilio Hernández-García, and Enrico Ser-Giacomi. 2017. Introduction to Focus Issue: Complex network perspectives on flow systems. *Chaos: An Interdisciplinary Journal of Nonlinear Science* 27, 3 (2017).
- [11] Sven Erlander and Neil F Stewart. 1990. *The gravity model in transportation analysis: theory and extensions*. Vol. 3. Vsp.
- [12] Karl J Friston, Maxwell JD Ramstead, Alex B Kiefer, Alexander Tschantz, Christopher L Buckley, Mahault Albarracín, Riddhi J Pitliya, Conor Heins, Brennan Klein, Beren Millidge, et al. 2024. Designing ecosystems of intelligence from first principles. *Collective Intelligence* 3, 1 (2024), 26339137231222481.
- [13] Marta C. González, César A. Hidalgo, and Albert-László Barabási. 2008. Understanding individual human mobility patterns. *Nature* 453 (2008), 779–782.
- [14] Stephen Hincks and Cecilia Wong. 2010. The spatial interaction of housing and labour markets: commuting flow analysis of North West England. *Urban Studies* 47, 3 (2010), 620–649.
- [15] Ibai Lana, Javier Del Ser, Manuel Velez, and Eleni I Vlahogianni. 2018. Road traffic forecasting: Recent advances and new challenges. *IEEE Intelligent Transportation Systems Magazine* 10, 2 (2018), 93–109.
- [16] Zhicheng Liu, Fábio Miranda, Weiting Xiong, Junyan Yang, Qiao Wang, and Cláudio T. Silva. 2020. Learning Geo-Contextual Embeddings for Commuting Flow Prediction. In *AAAI Conference on Artificial Intelligence*. <https://api.semanticscholar.org/CorpusID:211037977>
- [17] Scott M Lundberg and Su-In Lee. 2017. A unified approach to interpreting model predictions. *Advances in neural information processing systems* 30 (2017).
- [18] Yan Luo, Fu-lai Chung, and Kai Chen. 2022. Urban Region Profiling via Multi-Graph Representation Learning. In *Proceedings of the 31st ACM International Conference on Information & Knowledge Management (Atlanta, GA, USA) (CIKM '22)*. Association for Computing Machinery, New York, NY, USA, 4294–4298.
- [19] Yan Luo, Haoyi Duan, Ye Liu, and Fu-Lai Chung. 2023. Timestamps as Prompts for Geography-Aware Location Recommendation. In *Proceedings of the 32nd ACM International Conference on Information and Knowledge Management (<conf-loc>, <city>Birmingham</city>, <country>United Kingdom</country>, </conf-loc>)* (CIKM '23). Association for Computing Machinery, New York, NY, USA, 1697–1706.
- [20] Oisín Mac Aodha, Elijah Cole, and Pietro Perona. 2019. Presence-only geographical priors for fine-grained image classification. In *Proceedings of the IEEE/CVF International Conference on Computer Vision*. 9596–9606.
- [21] Gengchen Mai, Krzysztof Janowicz, Yingjie Hu, and Song Gao. 2018. ADCN: An anisotropic density-based clustering algorithm for discovering spatial point patterns with noise. *Transactions in GIS* 22, 1 (2018), 348–369.
- [22] Gengchen Mai, Krzysztof Janowicz, Bo Yan, Rui Zhu, Ling Cai, and Ni Lao. 2020. Multi-Scale Representation Learning for Spatial Feature Distributions using Grid Cells. In *International Conference on Learning Representations*.
- [23] Brian McKenzie. 2013. County-to-county commuting flows: 2006–10. *US Census Bureau* (2013).
- [24] OpenStreetMap contributors. 2017. Planet dump. <https://planet.osm.org>. Available online at <https://www.openstreetmap.org>.
- [25] N. Pourebrahim, S. Sultana, A. Niakanlahiji, and J.-C. Thill. 2019. Trip distribution modeling with Twitter data. *Computers, Environment and Urban Systems* 77 (2019), 101354.
- [26] Cynthia Rudin. 2019. Stop explaining black box machine learning models for high stakes decisions and use interpretable models instead. *Nature machine intelligence* 1, 5 (2019), 206–215.
- [27] Filippo Simini, Gianni Barlacchi, Massimiliano Luca, and Luca Pappalardo. 2021. A deep gravity model for mobility flows generation. *Nature communications* 12, 1 (2021), 6576.
- [28] Filippo Simini, Marta C González, Amos Maritan, and Albert-László Barabási. 2012. A universal model for mobility and migration patterns. *Nature* 484, 7392 (2012), 96–100.
- [29] Jungyul Sohn. 2005. Are commuting patterns a good indicator of urban spatial structure? *Journal of Transport geography* 13, 4 (2005), 306–317.
- [30] John Q Stewart. 1941. An inverse distance variation for certain social influences. *Science* 93, 2404 (1941), 89–90.
- [31] US Census Bureau. 2019. Longitudinal Employer-Household Dynamics. <https://lehd.ces.census.gov/data/>.
- [32] Ashish Vaswani, Noam Shazeer, Niki Parmar, Jakob Uszkoreit, Llion Jones, Aidan N Gomez, Łukasz Kaiser, and Illia Polosukhin. 2017. Attention is all you need. *Advances in neural information processing systems* 30 (2017).
- [33] Eleni I Vlahogianni, Matthew G Karlaftis, and John C Golias. 2014. Short-term traffic forecasting: Where we are and where we're going. *Transportation Research Part C: Emerging Technologies* 43 (2014), 3–19.
- [34] Jinwei Zeng, Guozhen Zhang, Can Rong, Jingtao Ding, Jian Yuan, and Yong Li. 2022. Causal Learning Empowered OD Prediction for Urban Planning. In *Proceedings of the 31st ACM International Conference on Information & Knowledge Management (Atlanta, GA, USA) (CIKM '22)*. Association for Computing Machinery, New York, NY, USA, 2455–2464. <https://doi.org/10.1145/3511808.3557255>
- [35] Peng Zhang, SC Wong, and SQ Dai. 2009. A conserved higher-order anisotropic traffic flow model: description of equilibrium and non-equilibrium flows. *Transportation Research Part B: Methodological* 43, 5 (2009), 562–574.
- [36] Zhilun Zhou, Jingtao Ding, Yu Liu, Depeng Jin, and Yong Li. 2023. Towards Generative Modeling of Urban Flow through Knowledge-enhanced Denoising Diffusion. *Proceedings of the 31st ACM International Conference on Advances in Geographic Information Systems* (2023). <https://api.semanticscholar.org/CorpusID:262054030>
- [37] Rui Zhu, Krzysztof Janowicz, and Gengchen Mai. 2019. Making direction a first-class citizen of Tobler's first law of geography. *Transactions in GIS* 23, 3 (2019), 398–416.
- [38] George Kingsley Zipf. 1946. The P 1 P 2/D hypothesis: on the intercity movement of persons. *American sociological review* 11, 6 (1946), 677–686.

Received 20 February 2007; revised 12 March 2009; accepted 5 June 2009